

Supporting Information

Enhanced Charge Storage of Ultrathin Polythiophene Films within Porous Nanostructures

*Siamak Nejati, Thomas E. Minford, Yuriy Y. Smolin, Kenneth K. S. Lau**

Department of Chemical and Biological Engineering, Drexel University

3141 Chestnut Street, Philadelphia, PA 19104, U.S.A.

Raman spectroscopy of polythiophene films

The Raman spectra of the film acquired at 488 nm showed a slight shift at 1500 cm^{-1} toward lower wavenumber indicative of higher conjugation length and differences in the $1000\text{-}1250\text{ cm}^{-1}$ region associated with highly doped polythiophene in the oxidized form when compared with the Raman spectra of the film deposited previously¹ using a different oxidant (vanadium oxytrichloride vs. antimony pentachloride). This behavior suggests that film has less defects when compared with the previously oCVD deposited film, which along with the red shift in the UV-vis signal is an indication of higher conjugation length in the deposited film. Also the deposited film using antimony pentachloride oxidant is highly doped which explains the higher conductivity of the as-deposited film. In order to obtain more structural information, Raman spectra were also acquired with a 633 nm laser. Figure S1 shows Raman spectra of the polythiophene films excited at 488 and 633 nm. Since undoped polythiophene films exhibit a very strong visible absorption band whose maximum is located anywhere between 470-520 nm that is related to the $\pi\text{-}\pi^*$ electronic transition (see Figure 1c in the main text), excitation at 488 nm preferentially enhances the Raman lines of this resonance of the undoped species and specifically the 1450 cm^{-1} which is assigned to the in-plane symmetric vibration of the thiophene ring.² We therefore chose to additionally excite at 633 nm to capture the doping effect with more accuracy by reducing biasing of the resonance related only to the undoped form. These results are in agreement with previous reports² on doped polythiophene excited at 633 nm and suggests that the oCVD deposition of polythiophene using SbCl_5 will generate a highly doped state of the as-deposited polymer. To investigate the effect of oCVD process parameters on polymer quality, the oxidant flow rate in the inlet stream was varied from 0.1 to 0.5 sccm while keeping other conditions constant (total pressure $P = 800$ mtorr, monomer flow rate $F_M = 2$ sccm stage temperature $T_s = 30$

°C). The Raman spectra of polythiophene deposited at three different oCVD conditions yielding different electrical conductivities ranging from 1 to 70 S/cm are shown in Figure S2. The intra C=C vibration corresponding to the quinoidic structure at $\sim 1420\text{ cm}^{-1}$ is observed to shift left as electrical conductivity increased.

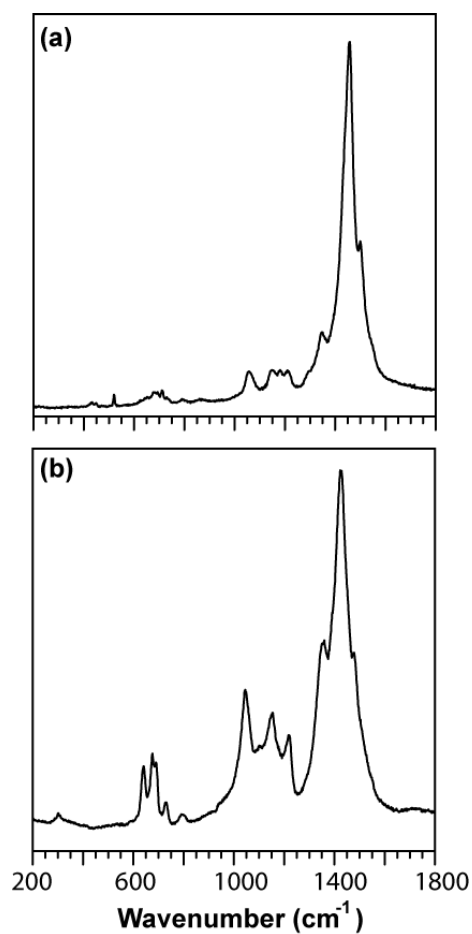


Figure S1. Raman spectra of polythiophene deposited on silicon, excited at (a) 488 nm and (b) 633 nm

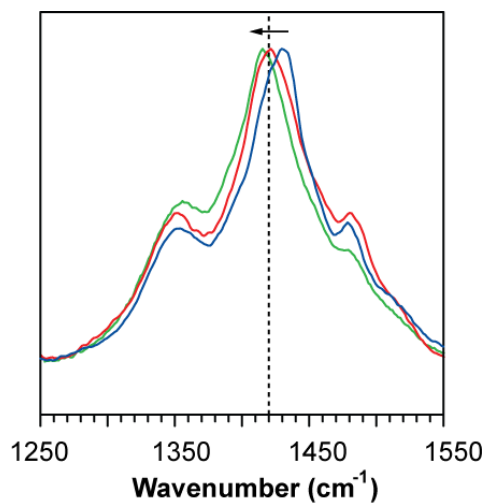


Figure S2. Raman spectrum of polythiophene deposited using different oCVD conditions, excited at 633 nm. The shift in the quinodonic peak to the lower wavenumber is concomitant with the increase in the film conductivity.

Conformal coating of polythiophene inside porous nanostructures

By enabling reaction limited conditions through control of oCVD process conditions, efficient mass transfer of reactant species leads to conformal coating of high aspect ratio nanoporous structures like the nanopores of anodized aluminum oxide (AAO) membranes. Conformal growth of the polymer with deposition rates as low as 0.5 nm/min (estimated from the average film thickness measured through SEM that was obtained over a certain deposition time) could be achieved as shown in Figure S3.

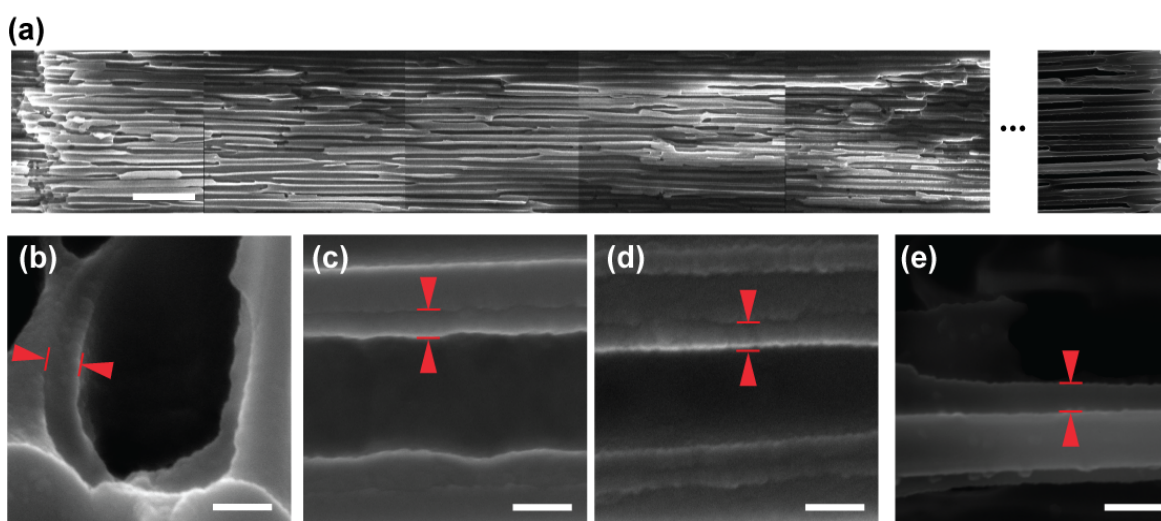


Figure S3. Conformal coating of polythiophene along the AAO membrane under reaction limited conditions. (a) SEM cross section of the AAO membrane at low magnification with leftmost being top and rightmost being bottom (scale bar is 2.5 μm). High magnification SEM showing uniform coating thickness at various positions in the AAO nanopores: (b) at the top, (c) 20 μm from the top, (d) 40 μm from the top, and (e) close to the bottom of the pore (scale bar is 50 nm).

To confirm the formation of polythiophene along the AAO nanopore wall, EDS mapping was performed on the cross section of the polythiophene-coated AAO. Both aluminum and sulfur signals were mapped, and as shown in Figure S4, the sulfur signal is present with uniform intensity along the cross section, which suggests uniform polythiophene coating. In contrast, as shown in Figure S5, under diffusion limited conditions where reaction is much faster (e.g. at high pressures greater than 800 mtorr or at high oxidant flow rates greater than 0.3 sccm) coating is confined mostly near the top of the membrane surface that leads instead to clogging of the pores.

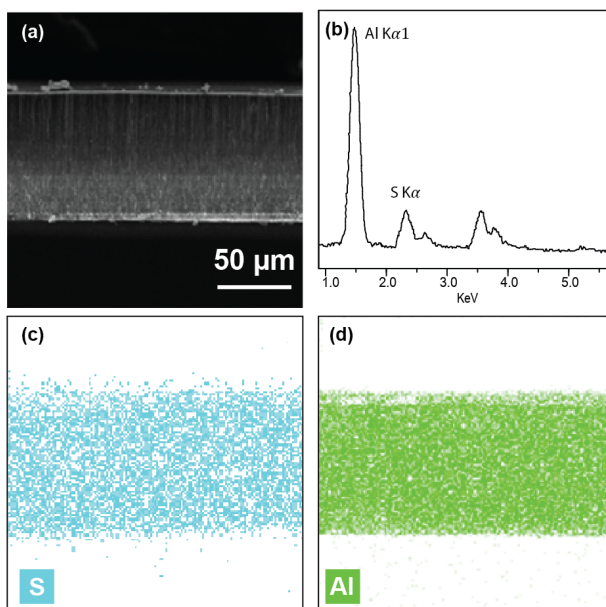


Figure S4. Energy dispersive x-ray spectroscopy over the cross section of polythiophene-coated AAO membrane. (a) SEM image of the AAO membrane, (b) representative EDS spectrum showing the aluminum and sulfur signals, (c) uniform sulfur intensity map along the cross section, and (d) uniform aluminum mapping along the cross section.

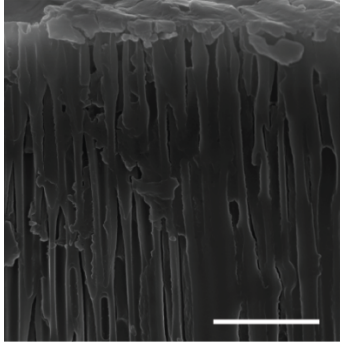


Figure S5. Cross sectional SEM of the AAO coated under diffusion limited conditions that resulted in pore blockage (scale bar is 500 nm).

We have applied our knowledge of the oCVD reaction space that governs the in-situ polymerization of polythiophene within well-defined AAO nanostructures to enable conformal coating within mesoporous TiO_2 layers supported on FTO glass. Since the porous nanostructure was more three-dimensional and the aspect ratio was even higher when compared with the AAO membrane, we had to increase the monomer flow rate from 2 to 4 sccm while reducing the total pressure from 800 to 500 mtorr to further reduce the rate of reaction within the TiO_2 pores effectively and thus allow efficient reactant mass transfer. This enabled conformal coating up to $4 \mu\text{m}$ of the TiO_2 layer thickness we tested. To confirm the formation polythiophene within the TiO_2 layer, EDS mapping was performed on the cross section of the polythiophene-coated TiO_2 mesoporous structure. Titanium, sulfur, tin and silicon indicative of TiO_2 , polythiophene, FTO and glass were mapped as can be seen in Figure S6. The uniform signal intensity of sulfur suggests that the polymer is conformally coated all the way to the bottom of the TiO_2 layer. Also, shown with the elemental mapping is the presence of the FTO and glass layers below the polythiophene-coated TiO_2 layer.

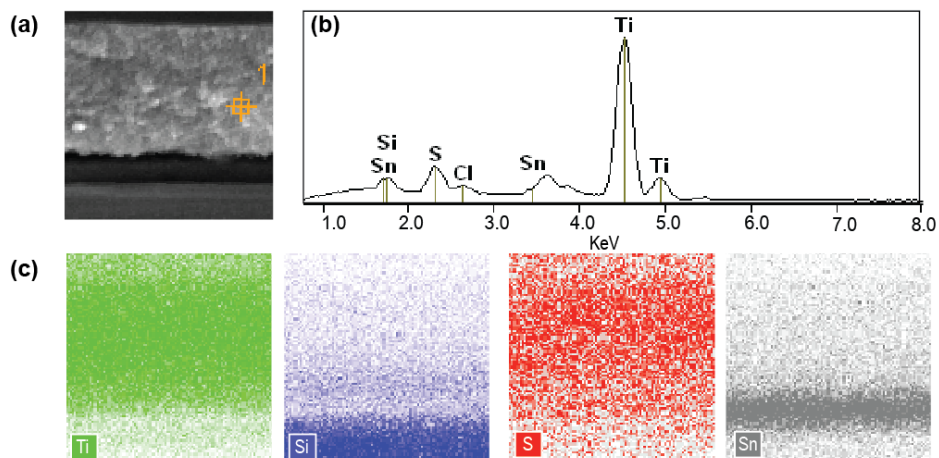


Figure S6. Energy dispersive x-ray spectroscopy over the cross section of polythiophene-coated mesoporous TiO_2 layers supported on FTO glass. (a) SEM image of the cross section, (b) representative EDX spectrum showing the titanium, sulfur, tin and silicon signals, indicative of TiO_2 , polythiophene, FTO, and glass, respectively, and (c) intensity maps of the respective elements along the cross section.

Cyclic voltammetry of polythiophene integrated within mesoporous TiO₂

As shown in Figure S7, the reversible electrochemical behavior of lightly coated polythiophene within the nanostructured TiO₂ electrode can be observed. As the scan rate is increased, the peak position at 0.78 V vs. Ag/AgCl remains unchanged. There is a slight indication of a double layer capacitance outside of the electrochemically active window of polythiophene from -1 to 0 V vs. Ag/AgCl. The fact that the uncoated TiO₂ porous layer itself had minimal measurable capacitance (< 1 F/g) for our case means that the minor charge storage contribution most likely comes from charge accumulated over the polymer in the form of a double layer capacitance.⁵ Typically, the double layer capacitance of TiO₂ is usually attributed to the defect sites on the surface that are hydroxylated⁶⁻⁸ and can go through charge and discharge in the same fashion that most hydrous metal oxides store charge.⁹ Here, using an aprotic solvent and also covering the surface with a semiconducting polymer can hinder this phenomenon. In addition, there is not a significant charge storage in between 0 and -0.5 V that is expected for TiO₂.⁸ This leads us to believe that the charge storage observed is related to the polythiophene and not of the underlying TiO₂ template.

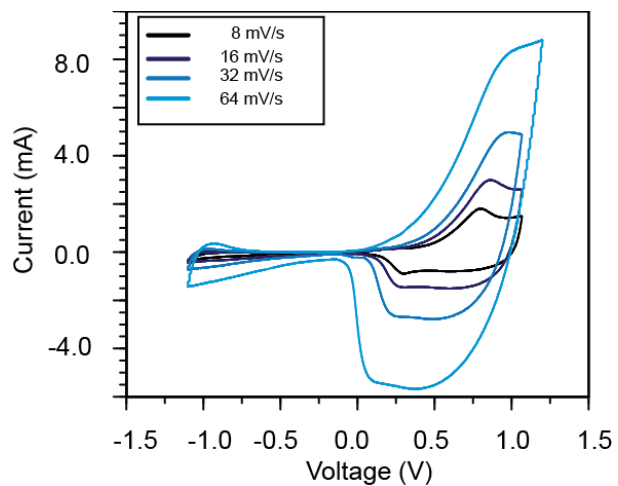


Figure S7. Cyclic voltammograms at different scan rates of polythiophene deposited within mesoporous TiO_2 electrodes recorded in a three electrode setup vs. an Ag/AgCl reference electrode.

Transmission electron microscopy of polythiophene integrated within activated carbon

STEM was performed on an activated carbon electrode that was lightly coated with polythiophene at a polymer-to-activated carbon mass ratio of ~ 0.75 . The sample was imbedded in epoxy resin and a diamond knife was used for microtomy. The resulting sample sectioned to ~ 100 nm thickness was viewed under TEM. As shown in Figure S8, the dark field TEM image and the EDS sulfur mapping suggest that the polymer is deposited within the activated carbon particle and not just residing on the external surface.

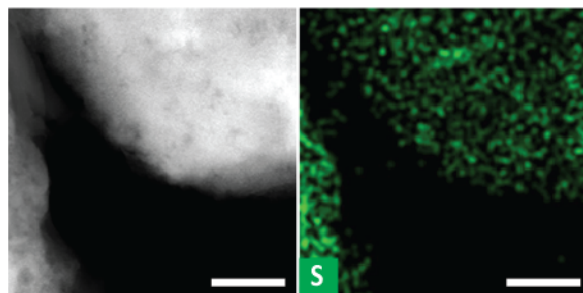


Figure S8. TEM image of a microtomed section of polythiophene-coated activated carbon electrode. (a) Dark field TEM, and (b) the sulfur signal from corresponding EDS analysis (scale bar is 150 nm).

References

1. Nejati, S.; Lau, K. K. S. Chemical Vapor Deposition Synthesis of Tunable Unsubstituted Polythiophene. *Langmuir* **2011**, *27*, 15223-15229.
2. Shi, G.; Xu, J.; Fu, M. Raman Spectroscopic and Electrochemical Studies on the Doping Level Changes of Polythiophene Films During Their Electrochemical Growth Processes. *J. Phys. Chem. B* **2001**, *106*, 288-292.
3. Asatekin, A.; Gleason, K. K. Polymeric Nanopore Membranes for Hydrophobicity-Based Separations by Conformal Initiated Chemical Vapor Deposition. *Nano Lett.* **2010**, *11*, 677-686.
4. Nejati, S.; Lau, K. K. S. Pore Filling of Nanostructured Electrodes in Dye Sensitized Solar Cells by Initiated Chemical Vapor Deposition. *Nano Lett.* **2011**, *11*, 419-423.
5. Peng, C.; Zhou, X.; Chen, G. Z.; Moggia, F.; Fages, F.; Brisset, H.; Roncali, Internally Referenced Analysis of Charge-Transfer Reactions in A New Ferrocenyl Bithiophenic Conducting Polymer through Cyclic Voltammetry. *Chem. Commun.* **2008**, 6606-6608.
6. Salari, M.; Aboutalebi, Chidembo, A. T.; Nevirkovets I. P.; S. H.; Konstantinov, K.; Liu, H. Enhancement of the Electrochemical Capacitance of TiO₂ Nanotube Arrays Through Controlled Phase Transformation of Anatase to Rutile. *Phys. Chem. Chem. Phys.* **2012**, *14*, 4770-4779

7. Lu, X.; Wang, G.; Zhai, T.; Yu, M.; Gan, J.; Tong, Y.; Li, Y. Hydrogenated TiO₂ Nanotube Arrays for Supercapacitors. *Nano Lett.* **2012**, *12*, 1690-1696
8. Wu, H.; Xu, J.; Lu, L.; Fan, Z.; Chen, X.; Song, Y.; Li, D. Enhanced Supercapacitance in Anodic TiO₂ Nanotube Films by Hydrogen Plasma Treatment. *Nanotechnology* **2013**, *24*, 455401.
9. Conway, B. E., *Electrochemical Supercapacitors: Scientific Fundamentals and Technological Applications*. Plenum: New York, 1999; pp 276-284.